Supplement material for

"Inconsistencies and Lurking Pitfalls in the Magnitude–Frequency Distribution of High-Resolution Earthquake Catalogs"

Marcus Herrmann, Warner Marzocchi

Description

The supplemental material complements our main paper with further information and results about inconsistencies in the MFD of HR catalogs. Most notably it (1) summarizes the inconsistencies in the MFD of the SCSN catalog, (2) shows the MFD analysis for the 1999 Hector Mine sequence, (3) illustrates the temporal dependence of the magnitude statistics for the Landers and Ridgecrest sequence (as done for L'Aquila in the main paper), and (4) demonstrates that sequence-based HR catalogs depart from an exponential-like MFD at a similar magnitude level as the network-based catalog even in a more complete period (without the evident short-term aftershock incompleteness, STAI).

This document contains:

- Text S1 and S2
- Figures S1 to S14 with captions

List of Figures

Text S1: Summary of inconsistencies in the MFD of the SCSN catalog due to different magnitude scales

- due to merging M_{L} and M_{w}:
  - 2019 Ridgecrest: at $\sim M3.5$, discontinuity due to the revised M_{L} (M_{Lr});
  - 2008–2017: at $\sim M4.4$, weak influence on b- and Lilliefors p-value;
  - 1999 Hector Mine: at$\sim M4.7$, too few events to see an effect;
  - 1992 Landers: at $\sim M4.7$, too few events;
- due to merging M_{coda} and M_{L}:
  - 1999 Hector Mine: between $\sim M2.0{-}2.5$, gradual merging, no evident discontinuity;
  - 1992 Landers: at $\sim M3.0$, strong discontinuity, especially due to added effect of M_{h});
- the M_{h} scale (helicorder/human/hand) scale is a particular case, which suffers from irregular binning intervals causing:
  1. major discontinuities due to the 0.5 binning at $M2.0$, 2.5, 3.0, and 3.5 until the 1999 Hector Mine sequence; and
  2. minor fluctuations due to the 0.1 binning until 2014 up to $M3.5$

Text S2: Analysis of magnitude statistics for the 1999 Hector Mine sequence

For the Hector Mine sequence we performed the same analyses as for the sequences in the main paper (see Fig. S3). Accordingly, we determined a $M_{\mathrm{c}}^{\mathrm{Lilliefors}} = 2.20$, which is not anymore caused by a discontinuity but mostly by the incompleteness; it is below $M_{\mathrm{c}}^{\mathrm{Lilliefors}}$ of the Landers sequence (3.01) due to the reduced contribution of the helicorder/human/hand magnitude, M_{h}, and coda amplitude magnitude, M_{coda}, above $M > 2$. Note that most of M_{h} for the Hector Mine sequence are below $\sim M1.8$ (see Fig. S3). The mixed binning of M_{h} still affects the b-value estimate (see Fig. S3b), albeit to a minor extent than for Landers; the largest bias exists at $M2.5$ and $M3.0$.

During the Hector Mine period, the fraction of M_{h} in the magnitude composition of the SCSN catalog is the largest among all investigated periods (see Fig. 4 in the main paper), which is mostly due to its over-proportional use for $M \lessapprox 1.8$ events (see Fig. S3).

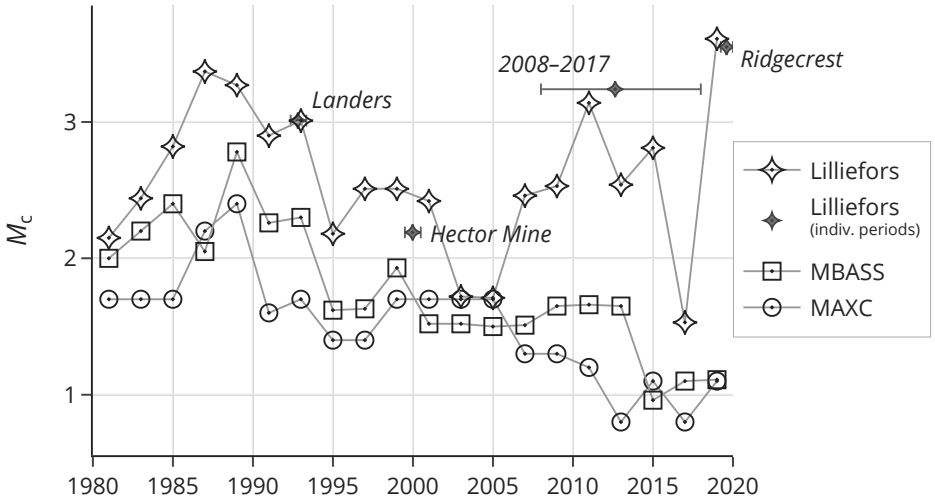

Figure S1: Time-dependent estimates of M_c using three different methods for the [*Hauksson et al.* 2012] catalog. Analogous to Fig. 5 in the main paper, but for *two*-year time intervals.

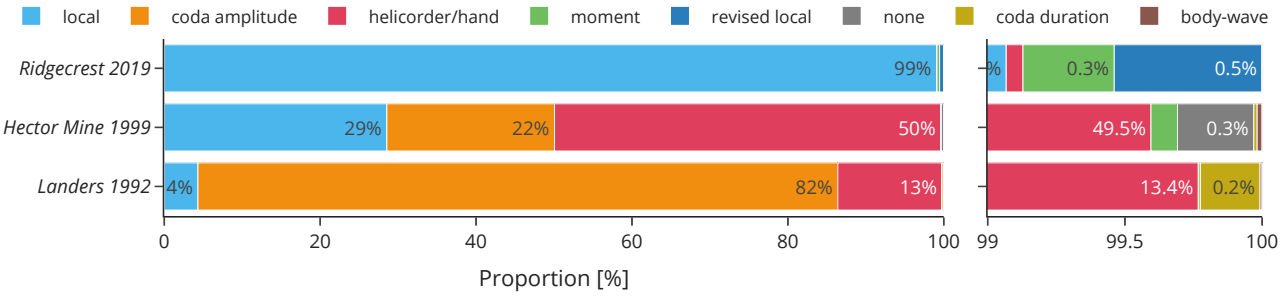

Figure S2: Analogous to Fig. 4 in the main paper, but using the USGS-ANSS ComCat: Proportion of magnitude types for different temporal periods of the catalog. Magnitude types are sorted by the order given in the legend. The right subfigure zooms into the 99–100% range. The proportions are essentially the same as in the SCSN catalog and differ only in a few minor aspects for older time periods: (1) in the Landers period the 'none' magnitude type is not present and it treats coda duration and body-wave magnitudes differently; (2) in the Hector Mine period the proportions differ by up to 1.4% and events with magnitude type 'none' in the SCSN catalog have empty values for the magnitude and magnitude type in the USGS-ANSS ComCat.

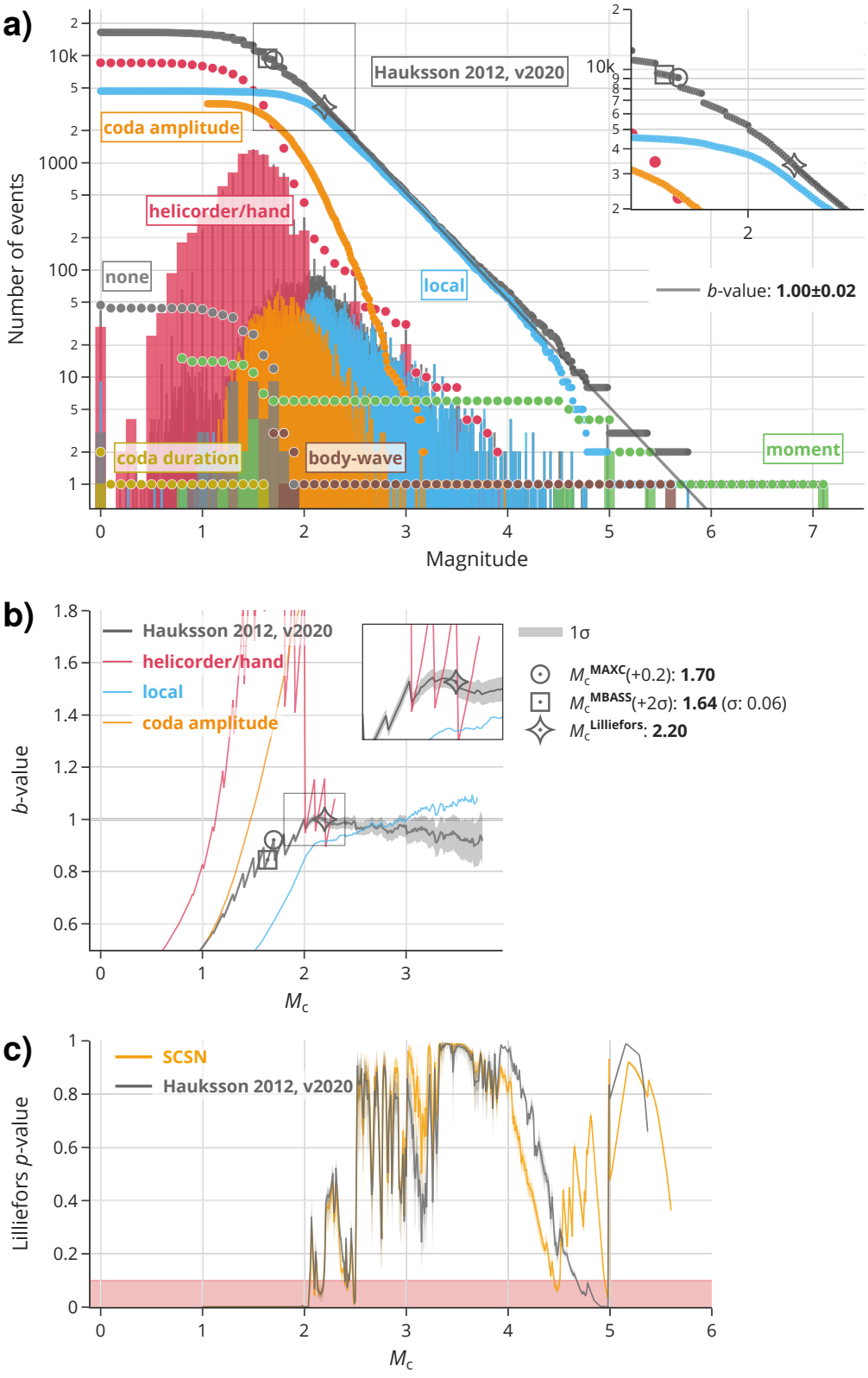

Figure S3: Analogous to Figs. 1, 2, 3, and 6 in the main paper but for the 1999 M7.1 Hector Mine sequence using one year of data (1999-07-01 until 2000-07-01, within 100 km from the mainshock).

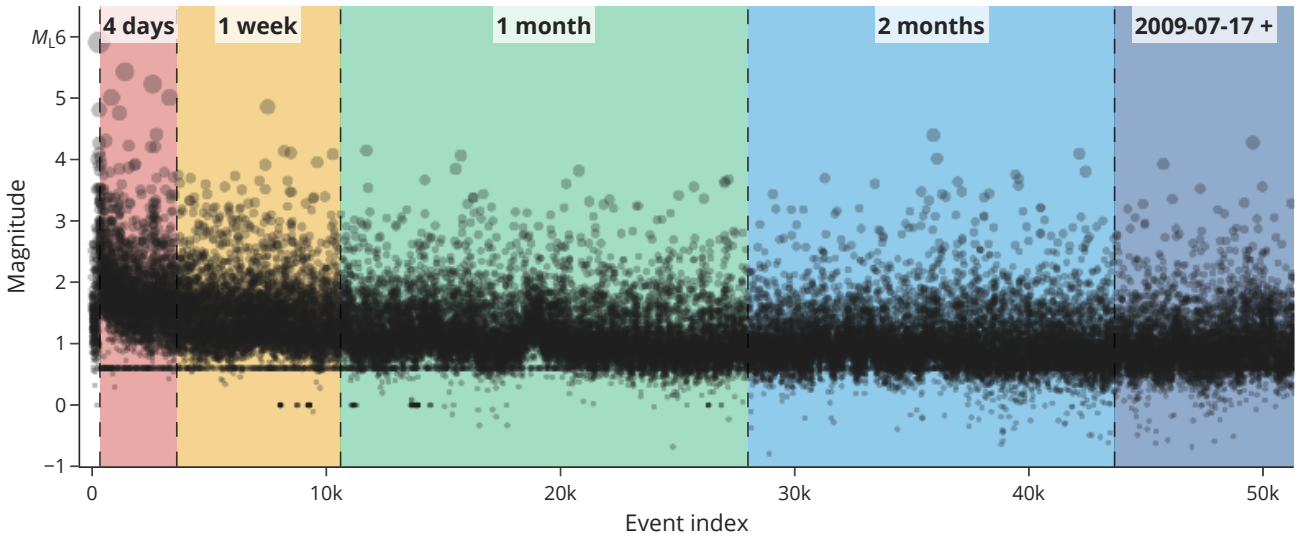

Figure S4: Equalized timeline of magnitudes as function of event number for the 2009 L'Aquila sequence using the *Valoroso et al.* [2013] catalog. The non-overlapping time windows used in Fig. 6 of the main paper are highlighted accordingly. The time range corresponds to 2009-01-07 until 2009-12-21.

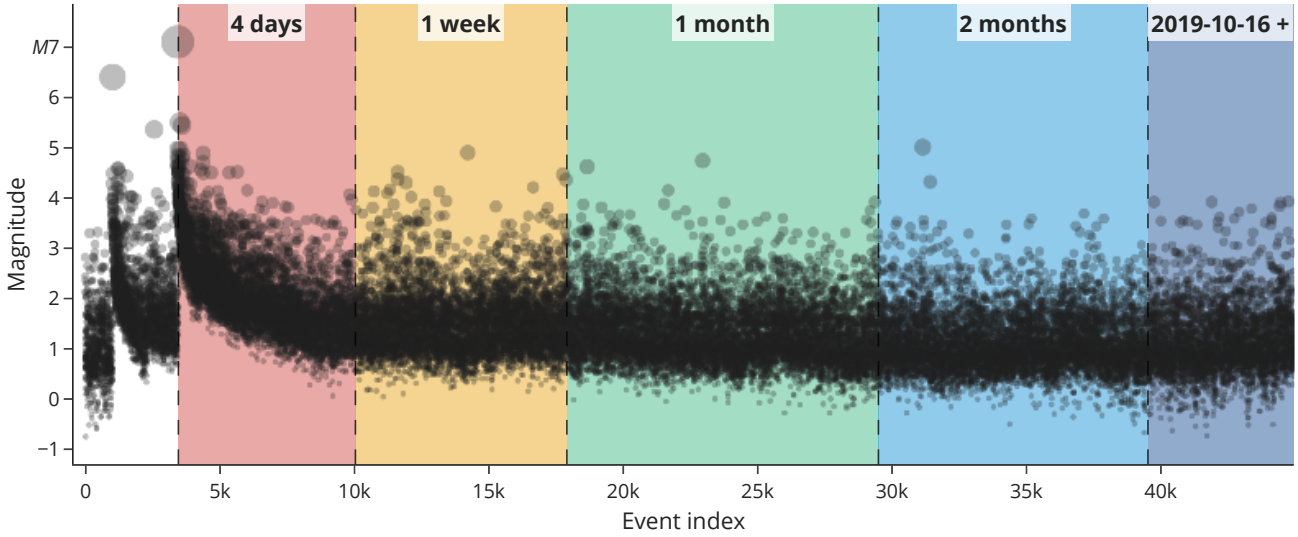

Figure S5: Equalized timeline of magnitudes as function of event number for the 2019 Ridgecrest sequence using the catalog of *Hauksson et al.* [2012] (2019-04-01 until 2019-12-31, 100 km from the mainshock). The highlighted non-overlapping time windows are used in Fig. S6.

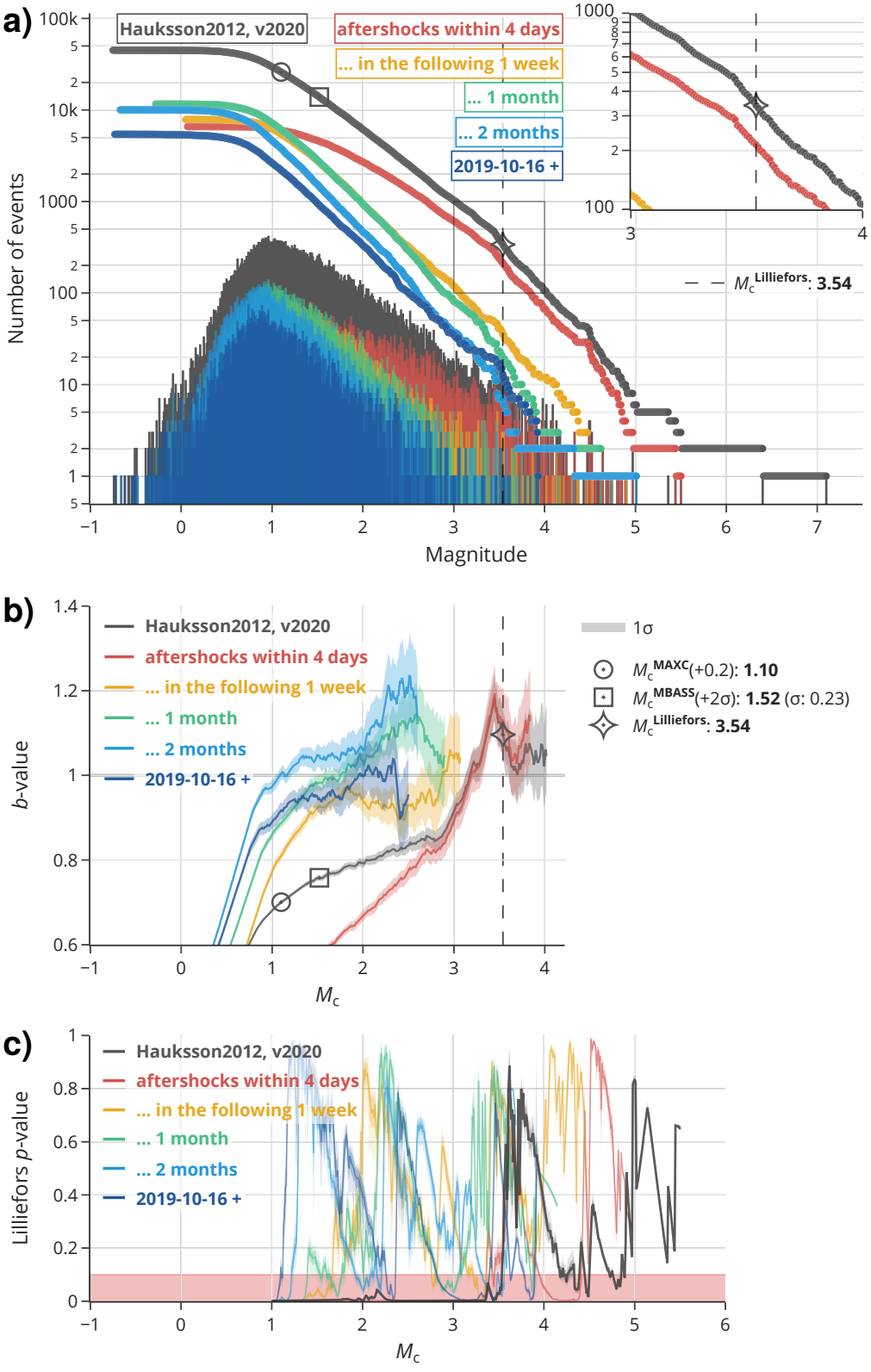

Figure S6: Analogous to Fig. 6 in the main paper but for the 2019 Ridgecrest sequence using non-overlapping time windows indicated in Fig. S5.

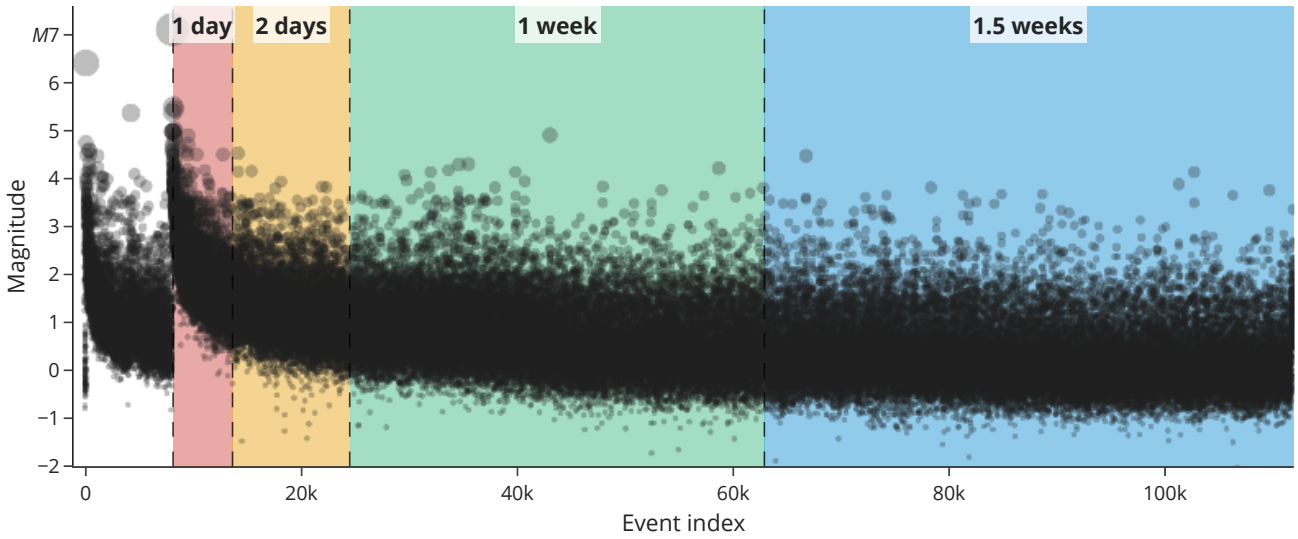

Figure S7: Equalized timeline of magnitudes as function of event number for the 2019 Ridgecrest sequence using the catalog of *Ross et al.* [2019] The highlighted non-overlapping time windows are used in Fig. S8. The time range corresponds to 2019-07-04 03:00 until 2019-07-25 15:00 UTC.

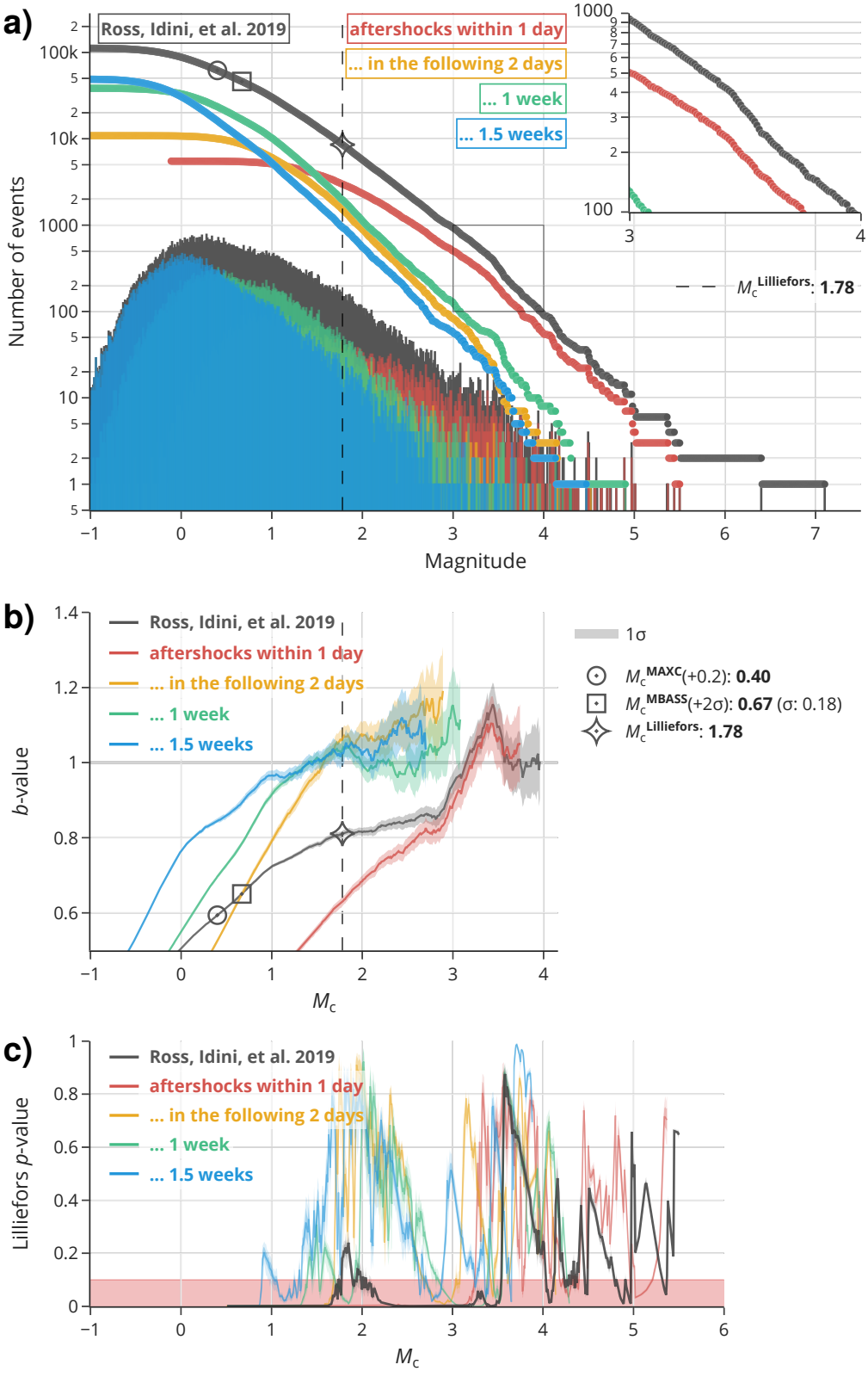

Figure S8: Analogous to Fig. S6 but for the catalog of *Ross et al.* [2019] using non-overlapping time windows indicated in Fig. S7.

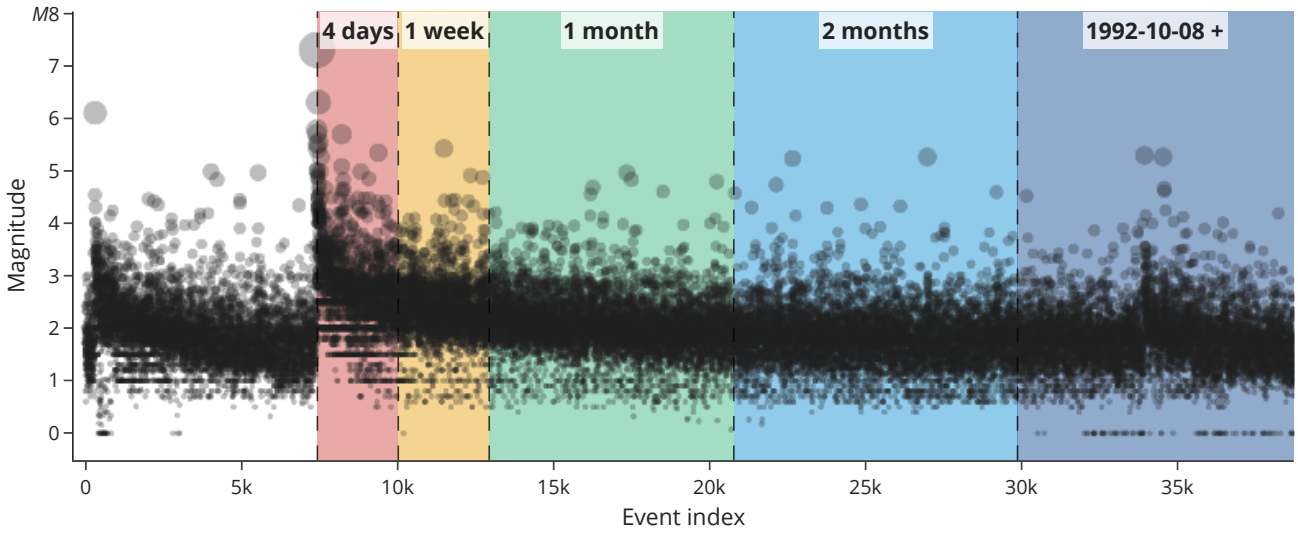

Figure S9: Equalized timeline of magnitudes as function of event number for the 1992 Landers sequence using the catalog of *Hauksson et al.* [2012] (1992-03-01 until 1993-02-28, 100 km from the mainshock). The highlighted non-overlapping time windows are used in Fig. S10.

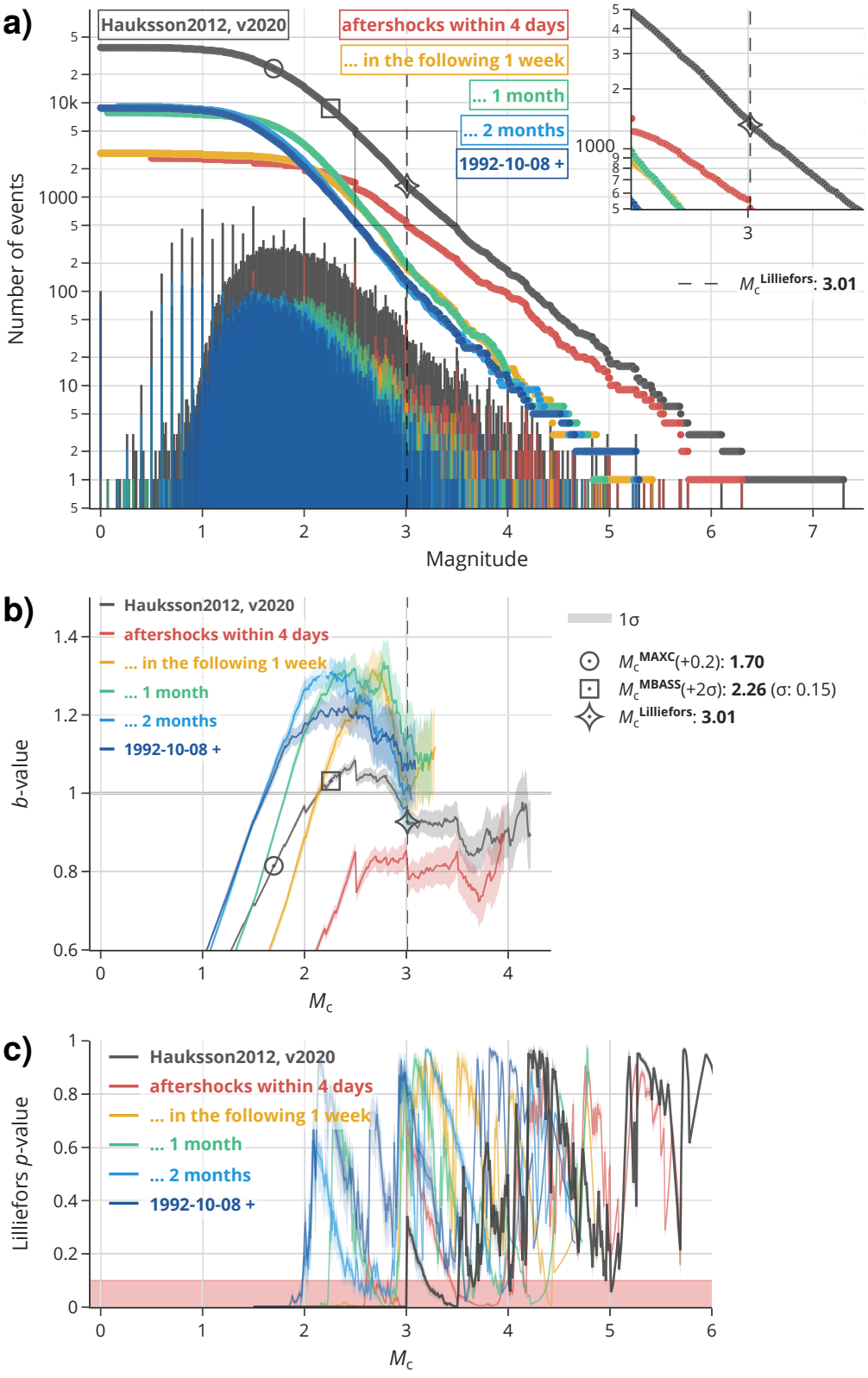

Figure S10: Analogous to Fig. 6 in the main paper and Fig. S6 but for the 1992 Landers sequence using non-overlapping time windows indicated in Fig. S9.

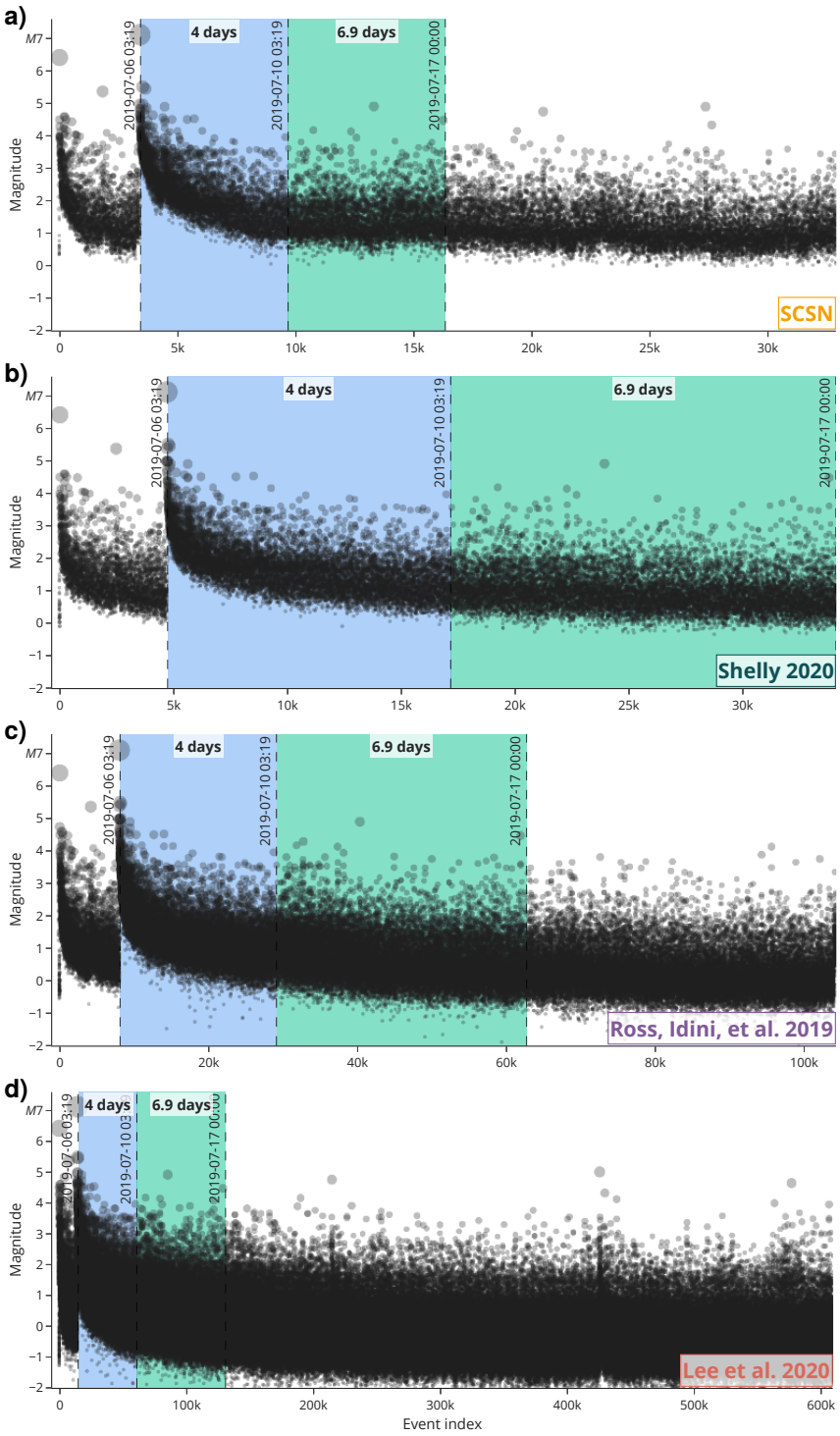

Figure S11: Equalized timelines of magnitudes as function of event number for the 2019 Ridgecrest sequence using the SCSN catalog (one-year extract as in Fig. S5) and the three template-matching-based catalogs *Ross et al.* [2019], *Shelly* [2020], and *Lee et al.* [2020] (see annotation in the lower right). The highlighted periods (blue and green) relate to the same time intervals. The duration of the first period (until 4 days after the *M*7.1 mainshock at 2019-07-06 03:19 UTC) was manually determined based on the SCSN catalog to exclude the evident short-term aftershock incompleteness (subfigure a; same as in Fig. S5) and applied to all other catalogs. The time span of the second period is limited by the end of the shortest catalog (2019-07-17 00:00 UTC of *Shelly* [2020]).

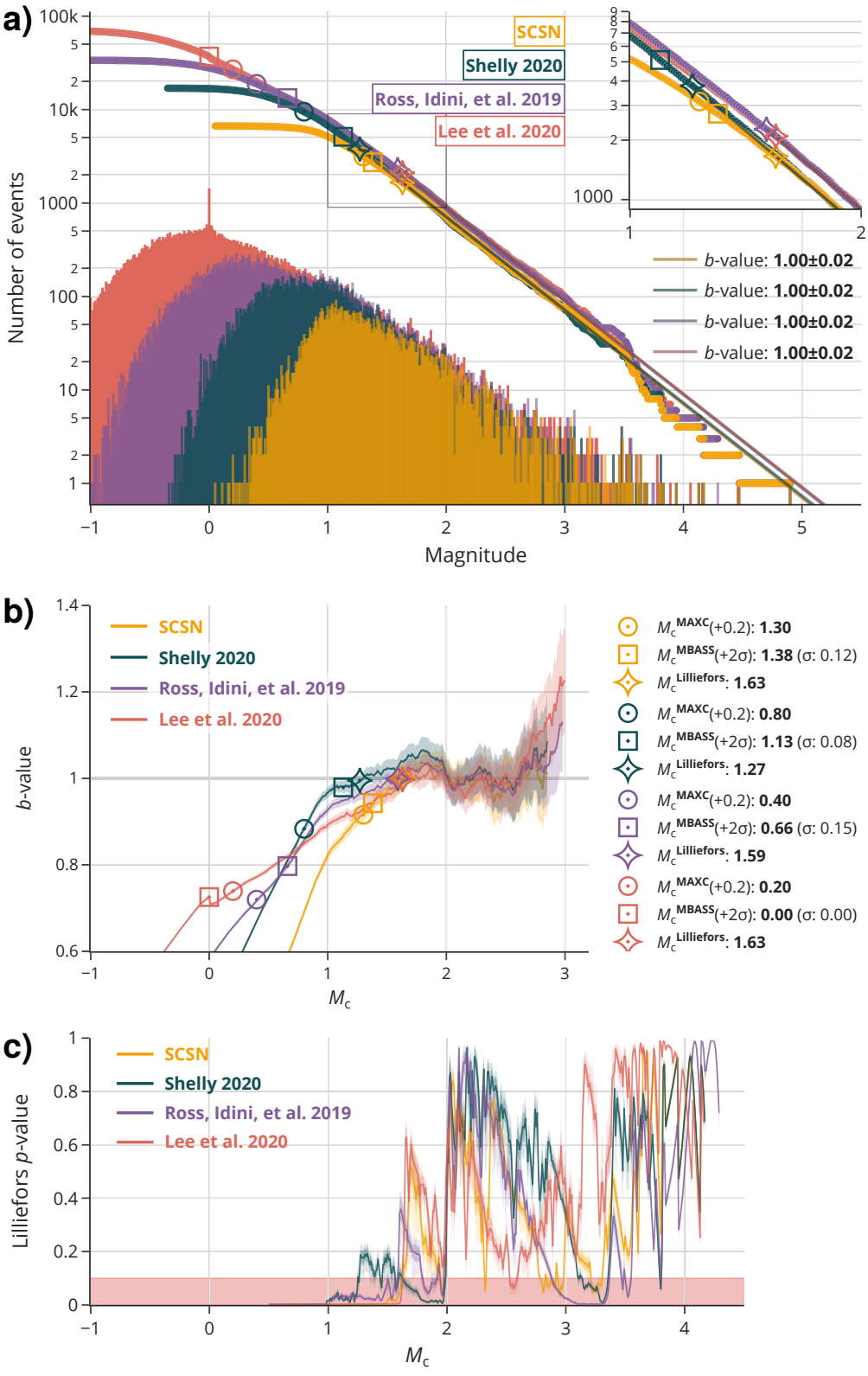

Figure S12: Analysis of magnitude statistics analogous to Fig. 1d–f for the catalogs shown in Fig. S11 using only the second period (highlighted in green).

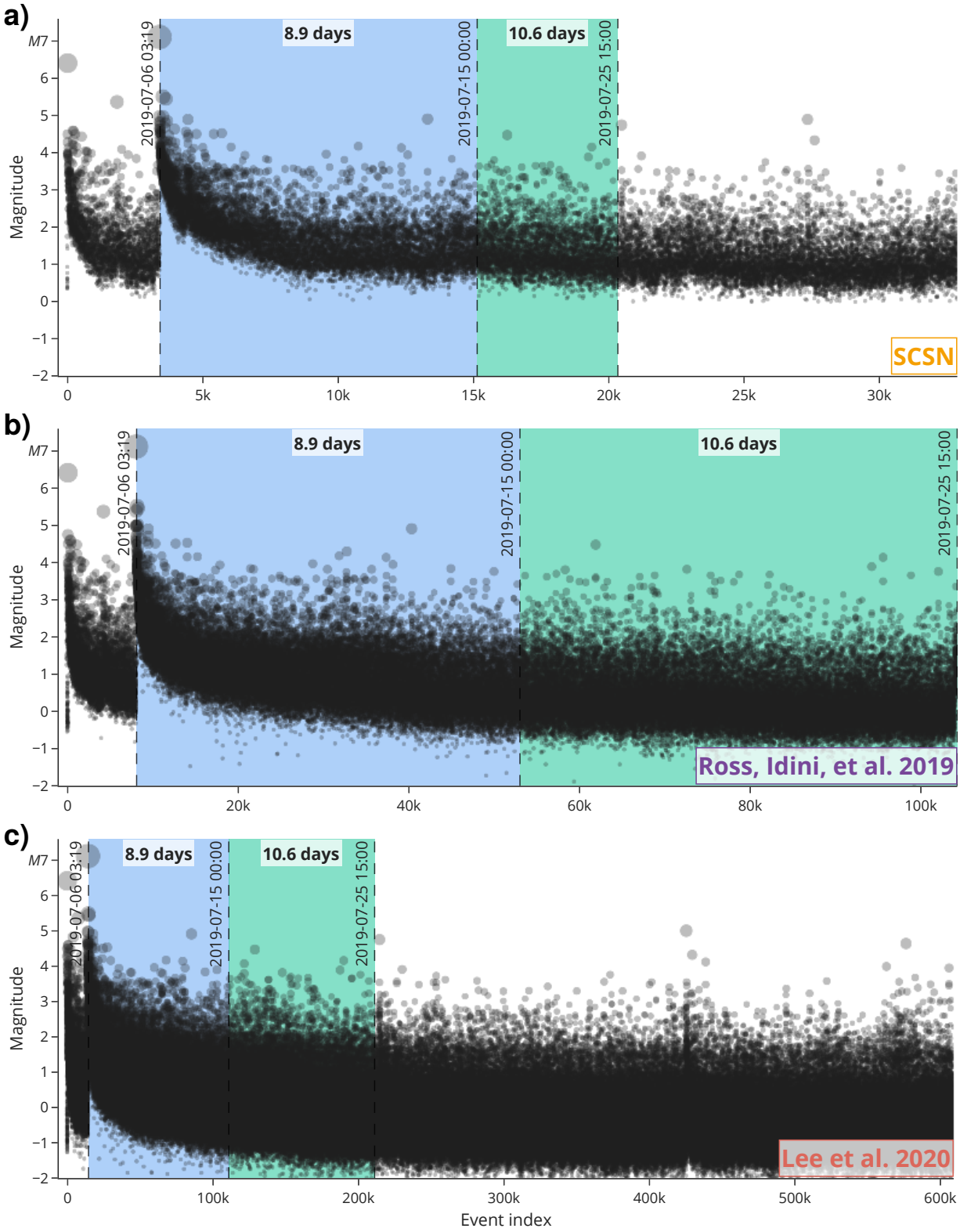

Figure S13: Analogous to Fig. S11, but with a more conservative consideration of the short-term incompleteness (starting ~9 days after the $M7.1$ mainshock). To include a reasonable amount of events, the catalog of *Shelly* [2020] was removed due to its limited duration; the time span of the second period (highlighted in green) is now limited by the end of the *Ross et al.* [2019] catalog (2019-07-25 15:00 UTC).

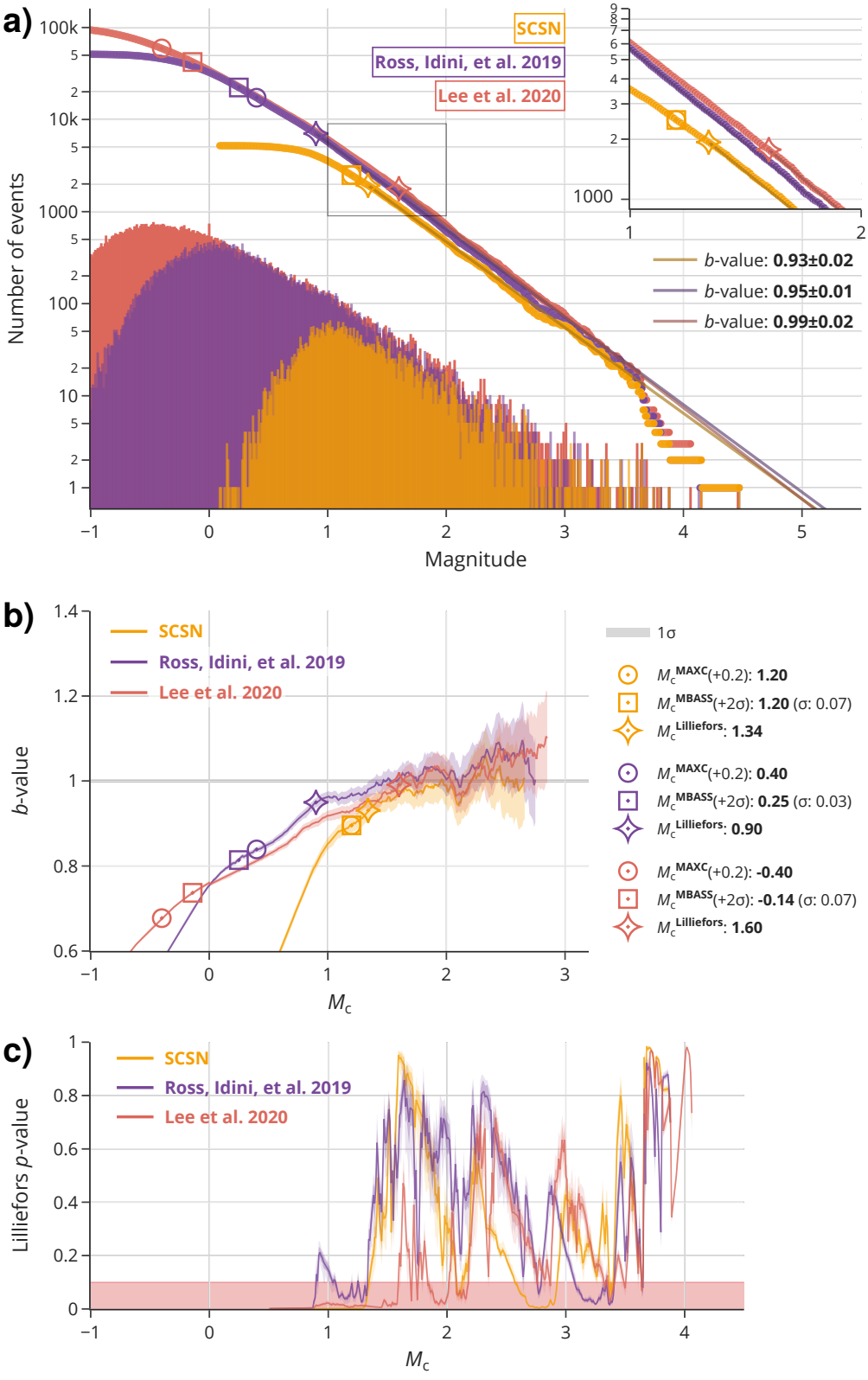

Figure S14: Analysis of magnitude statistics analogous to Fig. S12, but for the catalogs shown in Fig. S13 using only the second period (highlighted in green).

References

Hauksson, E., W. Yang, and P. M. Shearer (2012). "Waveform relocated earthquake catalog for Southern California (1981 to June 2011)". In: *Bulletin of the Seismological Society of America* 102.5, pp. 2239–2244. DOI: 10.1785/0120120010.

Lee, E.-J., W.-Y. Liao, D. Mu, W. Wang, and P. Chen (2020). "GPU-Accelerated Automatic Microseismic Monitoring Algorithm (GAMMA) and Its Application to the 2019 Ridgecrest Earthquake Sequence". In: *Seismological Research Letters* 91.4. DOI: 10.1785/0220190323.

Ross, Z. E. *et al.* (2019). "Hierarchical interlocked orthogonal faulting in the 2019 Ridgecrest earthquake sequence". In: *Science* 366.6463, pp. 346–351. DOI: 10.1126/science.aaz0109.

Shelly, D. R. (2020). "A High-Resolution Seismic Catalog for the Initial 2019 Ridgecrest Earthquake Sequence: Foreshocks, Aftershocks, and Faulting Complexity". In: *Seismological Research Letters* 91.4, pp. 1971–1978. DOI: 10.1785/0220190309.

Valoroso, L., L. Chiaraluce, D. Piccinini, R. Di Stefano, D. Schaff, and F. Waldhauser (2013). "Radiography of a normal fault system by 64,000 high-precision earthquake locations: The 2009 L'Aquila (central Italy) case study". In: *Journal of Geophysical Research: Solid Earth* 118.3, pp. 1156–1176. DOI: 10.1002/jgrb.50130.